ANL-6675

ANL-6675

Argonne National Laboratory

NUCLEATE BOILING CHARACTERISTICS AND THE CRITICAL HEAT FLUX OCCURRENCE IN SUBCOOLED AXIAL-FLOW WATER SYSTEMS

by

R. J. Weatherhead

ANL-6675
Engineering and Equipment
(TID-4500, 19th Ed.)
AEC Research and
Development Report

ARGONNE NATIONAL LABORATORY
9700 South Cass Avenue
Argonne, Illinois

NUCLEATE BOILING CHARACTERISTICS AND THE CRITICAL HEAT FLUX OCCURRENCE IN SUBCOOLED AXIAL-FLOW WATER SYSTEMS

by

R. J. Weatherhead

Reactor Engineering Division

March 1963

Operated by The University of Chicago
under
Contract W-31-109-eng-38
with the
U. S. Atomic Energy Commission

TABLE OF CONTENTS

LIST OF FIGURES

LIST OF FIGURES

NOMENCLATURE

D_B, r_b	Nucleate bubble-size characteristic, in.
D_e	Equivalent flow-channel diameter, in.
G	Coolant mass velocity, $lb/(hr)(ft^2)$
H	Local enthalpy, Btu/lb
H_f	Saturated liquid water enthalpy, Btu/lb
H_{fg}	Latent heat of vaporization, Btu/lb
P	System pressure, psia
P_w	Saturation pressure at the transfer-surface temperature, psia
Q''	Applied heat flux, $Btu/(hr)(ft^2)$
Q''_c	Critical heat flux, $Btu/(hr)(ft^2)$
T	Local water temperature, °F
T_f	Saturated liquid water temperature, °F
T_w	Local transfer-surface temperature, °F
v_g	Specific volume of saturated water vapor, ft^3/lb
v_{fg}	Specific volume change during vaporization, ft^3/lb
σ	Surface tension of liquid water, $lb_f/in.$
$(H_f - H)$	Subcooled water or wet-steam enthalpy difference, Btu/lb
$(P_w - P)$	Nucleate boiling excess pressure characteristic, psi
$(T_w - T_f)$	Nucleate boiling excess temperature characteristic, °F
(v_{fg}/H_{fg})	Inverse volumetric latent heat of water, ft^3/Btu

NUCLEATE BOILING CHARACTERISTICS AND THE CRITICAL HEAT FLUX OCCURRENCE IN SUBCOOLED AXIAL-FLOW WATER SYSTEMS

by

R. J. Weatherhead

ABSTRACT

An empirical analysis is used to equate the pressure term in the Jens-Lottes nucleate boiling wall superheat equation to the liquid coolant surface tension, which modifies the equation to

$$T_w - T_f = 0.18 \times 10^6 \sigma (Q''/10^6)^{1/4}$$

for surfaces of "average" nucleation capability. This equation is used to determine the pressure dependency of several nucleate boiling characteristics, including proportionate nucleate bubble sizes. The pressure dependency of the nucleate bubble-size characteristic is shown to be virtually identical with the pressure dependency of the mass-velocity term in the Jens-Lottes subcooled water critical heat flux correlation. Other alterations and additions are explained, and the modified form of the equation:

$$Q''_c/10^6 = \frac{2}{3} D_e^{-1/2} (H_{fg}/10^3)(G/10^6)^m \left[1 + \tanh \frac{H_f - H}{100} \right] ,$$

with $m = 0.175 \times 10^{-3} (v_{fg}/H_{fg})^{-1}$, is compared with data for circular and rectangular flow channels.

Several subcooled boiling flow regimes are hypothesized and explained to account for the unusual effect of the mass velocity upon the critical heat flux in the low-subcooling, low-steam-quality region. A pronounced surface effect, paralleling the nucleate boiling surface effect, upon the critical heat flux occurrence at the higher subcoolings is illustrated and used to explain apparent discrepancies within and among several representative bodies of critical heat flux data.

I. INTRODUCTION

In a forced-convection, axial-flow system, the heat transfer surface is separated from the coolant flow stream by a hydrodynamically established boundary layer. For nonboiling liquid coolants of low thermal conductivity, this boundary layer constitutes a limiting thermal barrier, and the heat transfer and flow friction of the system are determined by the velocity-dependent degree of turbulence existing at the interface between boundary layer and flow stream.

Nucleate boiling occurs when the transfer-surface temperature reaches a point sufficiently above the coolant saturation temperature to generate vapor bubbles in minute cavities (nucleation sites) on the heat transfer surface. The large increase in the interfacial turbulence caused by the expulsion of the nucleate bubbles through the boundary layer into the flow stream results in corresponding increases in the heat transfer and flow friction. The most simple form of nucleate boiling exists when the vapor bubbles are quenched or so absorbed by the flow stream or coolant medium as to have no further effect on the interfacial turbulence after the initial eruptive action. Examples of simple nucleate boiling are subcooled and saturated pool boiling from horizontal surfaces and highly subcooled forced-flow nucleate boiling.

Simple nucleate boiling is characterized by a fixed excess surface temperature which is dependent only on the applied heat flux, the pressure-dependent physical properties of the coolant, and the nucleating capability of the transfer surface. Its independence of the convective heat transfer criteria - the flow stream mass velocity and subcooling - can be inferred from experimental data and has been explained by Forster.[1] Convincing supplementary evidence of this is supplied by recent French data[2] which shows that the turbulence induced by the imposition of a high-potential, AC electrical field on a pool-boiling system has little effect on the nucleate boiling excess surface temperature and a definite beneficial influence on the convective transfer mechanisms of the nonboiling and film-boiling regions.

II. CHARACTERISTICS OF SIMPLE NUCLEATE BOILING

The excess surface temperature $(T_w - T_f)$ associated with simple nucleate-boiling water systems has been empirically defined by the Jens-Lottes[3] equation:

$$T_w - T_f = 60\, e^{-p/900}\, (Q''/10^6)^{1/4} \quad , \qquad (1)$$

the numerical coefficient and heat-flux dependency representing values for transfer surfaces of average "roughness." There is strong experimental evidence for a predominating surface dependency, the data of Berenson,[4]

for example, illustrating the effect rather conclusively. If we accept the transfer-surface roughness as a qualitative measure of the statistical average of the size and concentration of the bubble-nucleation sites, and recall from accepted nucleation theory[5] that the nucleate-bubble size is directly related to the size of the surface cavity in which it is formed, it may be concluded that the magnitude and heat flux dependency of the simple nucleate boiling excess surface temperature is determined by the number and size of the bubbles generated per unit of transfer surface area.

The Gibbs equation,

$$r_B = 2\sigma/(P_w - P) \quad , \tag{2}$$

relates the nucleate-bubble radius (r_B) to the excess pressure ($P_w - P$) which forms the bubble against the resisting force of the liquid surface tension (σ). If the excess surface temperature is considered to be the driving force required to generate the excess pressure, Eq. (2) shows that the magnitude of the excess surface temperature is inversely related to the nucleate-bubble size. The previously cited direct relationship between the bubble and surface cavity sizes leads to the conclusion that the magnitude of the excess surface temperature is inversely dependent upon the statistical size of the nucleation sites, and, by exclusion, that the heat flux dependency varies inversely as the concentration of the nucleation sites. (It should be borne in mind that the characteristic constant surface temperature measured during simple nucleate boiling is the integrated average of varying microscopically local temperatures over some finite area of the heat transfer surface.)

The liquid surface tension is also a determining factor in the nucleate-bubble size [Eq. (2)]. For water it can be expressed as a linear function of the coolant temperature:

$$\sigma = (500-0.707T)10^{-6} \text{ lb}_f/\text{in.} \tag{3}$$

Evaluated at the (Fahrenheit) saturation temperature and expressed as the equivalent saturation pressure, comparison (see Fig. 1) of the values of the surface tension with the pressure term ($e^{-P/900}$) of Eq. (1) leads to the modified form

$$T_w - T_f = 0.18 \times 10^6 \, \sigma(Q''/10^6)^{1/4} \quad . \tag{4}$$

The quantitative classification of transfer-surface nucleation capability being considerably beyond the scope of this discussion, the coefficient and heat flux dependency of Eq. (4) are based on the corresponding terms in Eq. (1). On a qualitative basis, experimental data show that finely grained surfaces (such as stably corroded stainless steel) have good nucleating capability whereas highly polished surfaces perform poorly.

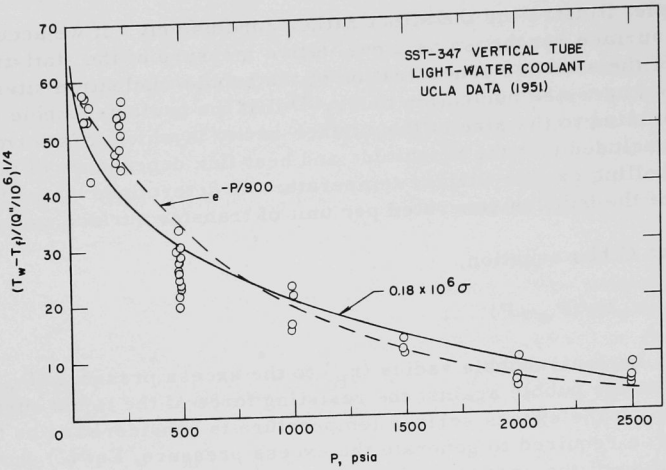

Fig. 1. Comparison of Values of Surface Tension with the Pressure Term of Eq. (1) for Nucleate Boiling Excess Surface Temperature.

Accepting the fixed excess surface temperature of Eq. (4) as an identifying characteristic of simple nucleate boiling, the equivalent excess pressure deriving from it may also be considered as characteristic, having a proportional validity rather than numerical accuracy. This proportionality is a result of the fact that T_w is an integrated average of the varying microscopically local values. A plot of the excess pressure characteristic as a function of system pressure (see Fig. 2) yields a curve closely paralleling the Zuber-Tribus[6] equation for the critical heat flux during the pool boiling of saturated water. If pressure-dependent changes in the resisting forces are neglected, the bubble discharge velocity (from the boiling surface) should be proportional to the driving force of the excess pressure characteristic; in a system which is not complicated by the presence of flow or subcooling effects, the limiting value of nucleate boiling (the critical heat flux occurrence) has a pressure dependence determined by the escape velocity of the nucleate bubbles.

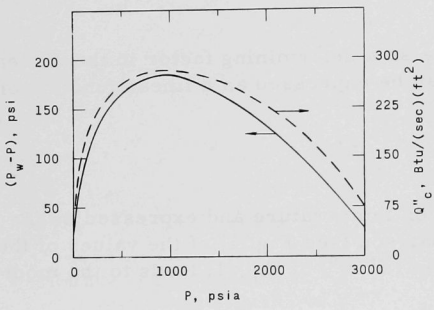

Fig. 2. Similarity between Nucleate Boiling Excess Pressure Characteristic $P_w - P$ and the Zuber-Tribus Equation for Critical Heat Flux Q_c'' during Pool Boiling of Saturated Water.

Values for the nucleate-bubble size calculated from Eq. (2) are patently absurd, but the pressure dependency has a proportional validity equal to the excess pressure characteristic used in the computation. Figures 3, 4, and 5 show the variation of this nucleate-bubble characteristic with system pressure and pertinent pressure-dependent properties of the coolant.

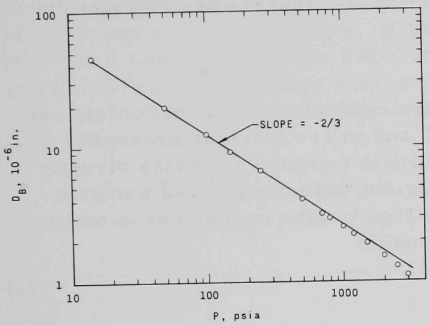

Fig. 3

Variation of Nucleate-bubble-diameter Characteristic D_B with System Pressure P for Water.

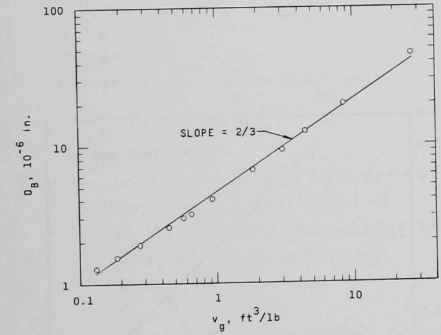

Fig. 4. Variation of Nucleate-bubble-diameter Characteristic D_B with Specific Volume of Saturated Water Vapor, v_g.

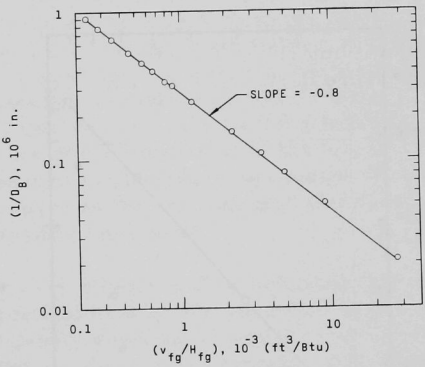

Fig. 5. Variation of Inverse Nucleate-bubble-diameter Characteristic $1/D_B$ with Inverse Volumetric Latent Heat of Water, v_{fg}/H_{fg}.

III. CRITICAL HEAT FLUX

The limiting value of nucleate-boiling intensity - the critical heat flux occurrence - is reached when the predominantly liquid boundary layer flashes to the vapor phase. In simple nucleate boiling, this reversion to a low-effeciency convective heat transfer mechanism is characterized by an

extreme and abrupt temperature excursion of the transfer surface and an equally precipitous reduction in coolant flow as the volumetric change of the flashing boundary layer exerts a throttling action on the flow channel.

Unlike the simple nucleate-boiling characteristics, the critical heat flux occurrence in subcooled water-flow systems shows a definite dependence on the convective transfer criteria of mass velocity and local coolant enthalpy. This dependency is expressed in the Jens-Lottes[3] equation:

$$Q''_c/10^6 = C(G/10^6)^m (T_f - T)^{0.22} \quad , \tag{5}$$

which is an empirical expression for the critical heat flux occurrence in axial-flow subcooled water systems; C and m are given as pressure-dependent numerical values. The fractional exponent m varies directly with the system pressure, and a comparison with the inverse nucleate-bubble-size characteristic is shown in Fig. 6. The agreement is exceptionally good, but a more useful relationship

$$m \approx 0.175 \times 10^{-3} (v_{fg}/H_{fg})^{-1} \tag{6}$$

with the volumetric latent heat of vaporization is illustrated in Fig. 7.

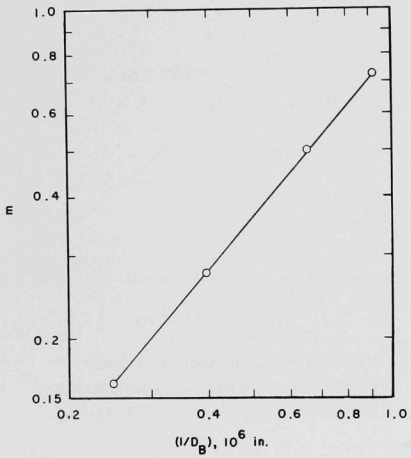

Fig. 6. Similarity between Inverse Nucleate-bubble Characteristic $1/D_B$ and the Pressure-dependent Mass-velocity Exponent m in Eq. (5).

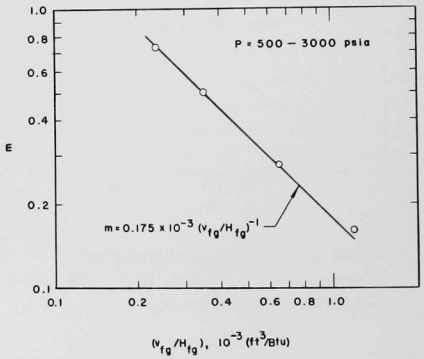

Fig. 7. Comparison of Empirical Values of Pressure-dependent Mass-velocity Exponent m in Eq. (5) with the Inverse Volumetric Latent Heat of Water, v_{fg}/H_{fg}.

For water at a pressure just below the critical, m has a numerical value approaching 0.80, the commonly accepted value for the mass-velocity effect in nonboiling convective heat transfer. The turbulence factor represented by the mass-velocity exponent m can be considered a method of compensating for the decreasing mixing action of the nucleate-boiling process as the nucleate-bubble size decreases with increasing system pressure. As a consequence of this decrease of boiling turbulence, the mass-velocity turbulence becomes of increasing importance, reaching its full nonboiling effect at the critical pressure. If we consider the total interfacial turbulence as a summation of the relatively constant mass-velocity turbulence and the pressure-dependent nucleate-boiling turbulence, its qualitative contribution to the pressure-dependent decrease in the critical heat flux is readily apparent.

Theoretical analyses[6] of subcooled and saturated pool-boiling systems show a direct proportionality between the critical heat flux and the latent heat of vaporization. A comparison of the values of the coefficient C of Eq. (5) and the latent heat of water is shown in Fig. 8. The approximate linear proportionality is far from conclusive, but consideration of the latent heat as a measure of the thermal transport associated with the nucleate-boiling process indicates a directly proportional relationship. If this be used as a working hypothesis, the contribution of the latent heat to the pressure-dependent decrease in the critical heat flux is also readily apparent.

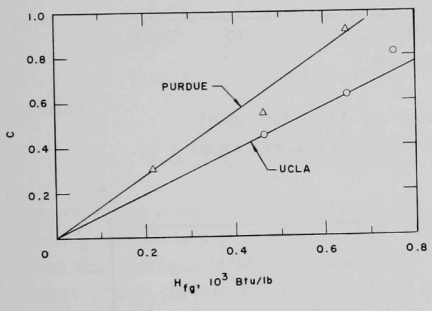

Fig. 8. Comparison of Pressure-dependent Coefficient C in Eq. (5) with the Latent Heat of Vaporization of Water, H_{fg}.

Figure 8 also indicates that the critical heat flux occurrence is inversely dependent upon the diameter of the flow channel. A similar dependency, under more closely controlled conditions and of more conclusive result, is shown in Fig. 9. The previously demonstrated effect of other convective criteria - mass velocity and coolant subcooling - lends added credibility to this experimental evidence. Empirical correlation of this presumed variable (see Fig. 10) over a rather narrow range of diameters indicates that the critical heat flux varies as the inverse square root of the diameter of the flow channel.

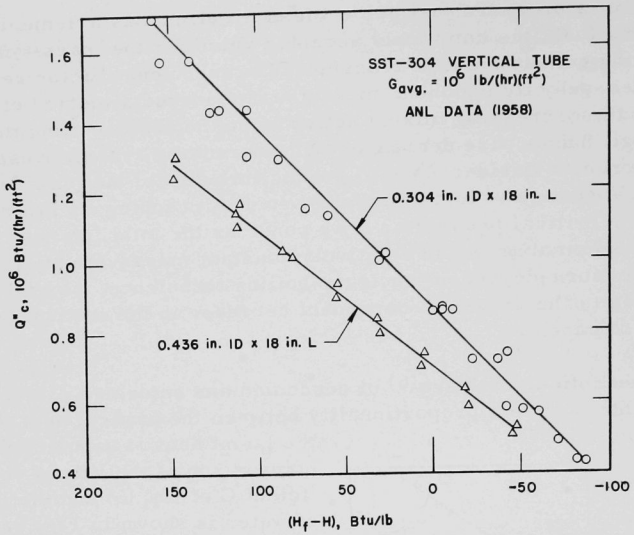

Fig. 9. Effect of Diameter of Flow Channel on Critical Heat Flux Occurrence at 2000 psia.

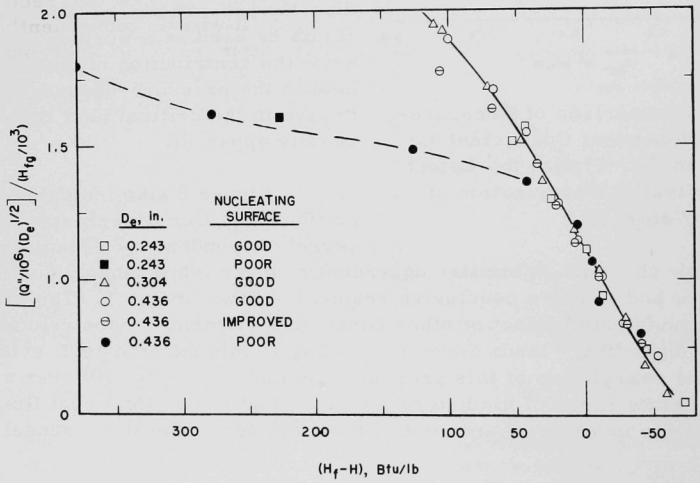

Fig. 10. Effect of Transfer-Surface Nucleation Capability upon Critical Heat Flux Occurrence at 2000 psia and Mass Velocity of 1.5×10^6 lb/(hr)(ft^2).

Figure 10 also shows the decided influence of the transfer-surface nucleation capability, the initially clean, smooth-drawn transfer surface being progressively corroded by repeated occurrences of the critical heat flux. The appearance of the dominant nucleate-boiling determinant in the limiting value of the nucleate-boiling process should not be particularly surprising. The apparent cessation of the surface effect in the low subcooling region is noteworthy, the pool boiling data of Berenson[4] showing a similar absence of surface effect at the saturation condition.

The empirical subcooling term of Eq. (5) is an adequate representation of the data upon which the correlation is based, but it has the obvious disadvantage of expressing a critical heat flux of zero at and beyond the saturated liquid condition. To avoid this difficulty, the subcooling term is replaced by a hyperbolic tangent function of the saturated enthalpy difference, $H_f - H$, on the purely arbitrary basis of similarity.

The modified form of Eq. (5) is

$$Q''_c/10^6 = \frac{2}{3} D_e^{-1/2} (H_{fg}/10^3)(G/10^6)^m \left[1 + \tanh \frac{H_f - H}{100}\right] , \qquad (7)$$

where

$$m = 0.175 \times 10^{-3} (v_{fg}/H_{fg})^{-1} .$$

Error-plot comparisons of Eq. (7) with data from circular and rectangular flow geometries are shown in Figs. 11 to 14. It will be subsequently shown that the surface effect and a lower limit on the mass velocity accounts for most of the deviation appreciably above the ±20% error band.

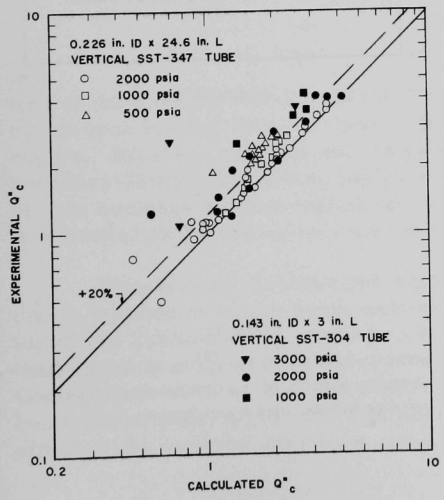

Fig. 11

Comparison of UCLA and Purdue Data[3] with Eq. (7) for Critical Heat Flux Occurrence in Subcooled Water Systems.

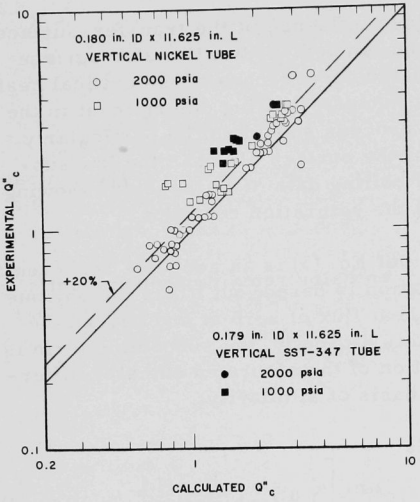

Fig. 12

Comparison of 1954 ANL Data[7] with Eq. (7) for Critical Heat Flux Occurrence in Subcooled Water Systems.

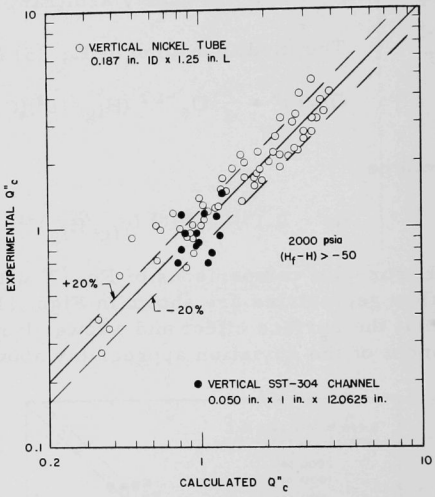

Fig. 13

Comparison of WAPD Data[8] for Circular and Rectangular Flow Geometries with Eq. (7) for Critical Heat Flux Occurrence in Subcooled Water Systems.

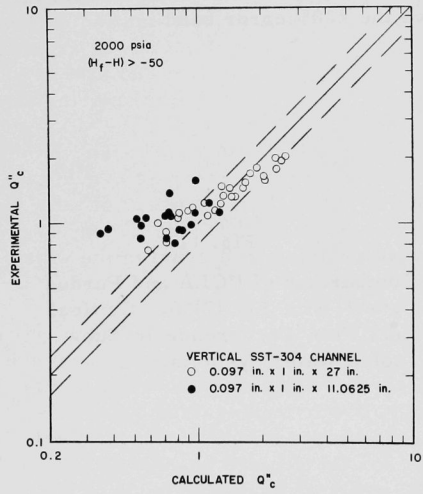

Fig. 14

Comparison of WAPD Data[8] for Rectangular Flow Geometry with Eq. (7) for Critical Heat Flux Occurrence in Subcooled Water Systems.

IV. EFFECT OF SUBCOOLED FLOW REGIME ON CRITICAL HEAT FLUX

Figure 10 shows a subcooling threshold above which there is a pronounced separation in the data from arbitrarily defined "good" and "poor" nucleating surfaces, the "good" surface data showing a predominant and approximately linear enthalpy dependency. The recent data of Silvestri[9] show that the local enthalpy remains predominant throughout the bubble and annular flow regimes of the wet-steam region and is accompanied by a reversal of the mass-velocity effect. A similar reversal of the mass-velocity influence is illustrated in Fig. 15. A similar inversion in the nucleate-boiling heat transfer at low subcoolings has been observed, the nucleate-boiling excess surface temperature increasing above its characteristic fixed level at high mass velocity [$G \approx 11 \times 10^6$ lb/(hr)(ft^2)] and decreasing slightly at lower velocities [$G \approx 1 \times 10^6$ lb/(hr)(ft^2)]. The beginning of this gradual reversal and subsequent stabilization of the mass-velocity effect on the critical heat flux occurrence and excess surface-temperature characteristic coincides roughly with the cessation of the surface effect. Sher[10] reports a parallel inverse mass-velocity effect upon boiling flow-friction in the low-subcooling, low-steam-quality region. All these changes can be related to changes in the effect of the boundary-layer turbulence, and it is apparent that the surface-dependent, simple nucleate boiling regime has been supplanted by a new regime which is adversely affected by increasing mass velocity.

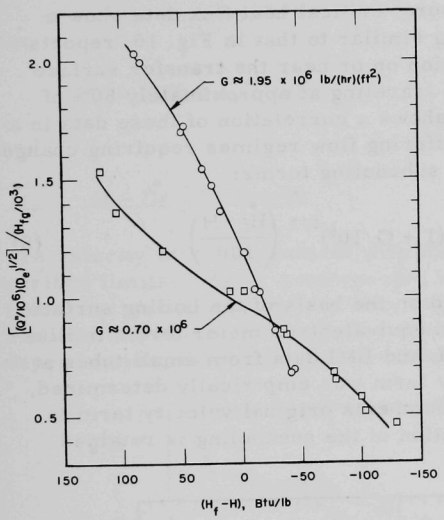

Fig. 15. Inversion of Mass-velocity Effect at 2000 psia in a Vertical SST-304 Tube (of 0.304-in. ID)

This boiling bubble-flow regime may be described as discrete nucleate bubbles of vapor in the subcooled or saturated liquid coolant, quenching of the bubbles being prevented by their proximity to the heating surface, inadequate mixing, or an inadequate liquid-vapor temperature difference. Containment of these bubbles within the flow stream apart from the interfacial turbulence region will not account for the decided changes in the effect of the several variables cited. An explanation can be found on the

basis of a stratified bubble flow, the separative action of the flow-stream-velocity profile tending to segregate the bubbles in a sub-boundary layer adjacent to the zone of interfacial turbulence. With the degree of segregation increasing directly with mass velocity, the sub-boundary bubble layer increasingly absorbs the mixing action of the nucleation turbulence, with resulting decreases in the heat transfer, critical heat flux, and flow friction.

Gunther,[11] whose low-pressure, critical heat flux data show a steep dependency on linear subcooling similar to that in Fig. 10, reports visual observation of bubble segregation on or near the transfer surface at high local subcoolings, the bubbles traveling at approximately 80% of the flow stream velocity. Figure 16 shows a correlation of these data in a form similar to that of Eq. (7), the differing flow regimes requiring changes in the coefficient, mass velocity, and subcooling terms:

$$Q''_c/10^6 = 1.75\, D_e^{-1/2}\,(H_{fg}/10^3)(1 + G/10^6)^{1/2}\left(\frac{H_f - H}{100}\right) \quad . \qquad (8)$$

With the equivalent diameter evaluated on the basis of the boiling surface only, the validity of the latent heat and equivalent-diameter terms is illustrated by the comparison with the ANL and BMI data from small tubes at 200 and 2000 psia. The mass-velocity term was empirically determined, and its proportional difference from Gunther's original velocity term is generally small; the linear approximation of the subcooling is retained from the original.

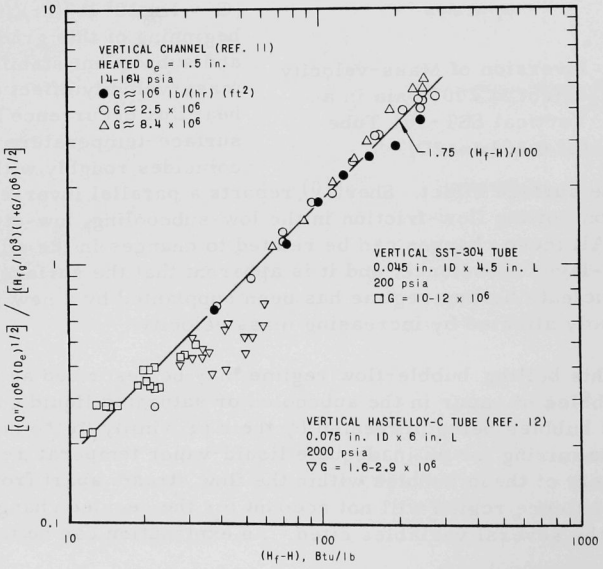

Fig. 16. Comparison of Low- and High-pressure Critical Heat Flux Data with Eq. (8)

An apparent pressure influence on the stratified bubble-flow-regime critical heat flux occurrence appears in the correlation of the 1958 ANL data shown in Fig. 17. The correlation is generically similar to Eq. (7) and (8):

$$Q''_c/10^6 = \frac{2}{3} D_e^{-1/2} (H_{fg}/10^3)(1 + G/10^6)^{1/2} \left[1 + \tanh \frac{H_f - H}{100} \right] , \quad (9)$$

for

$$G \geq 0.90 \times 10^6 \text{ lb/(hr)(ft}^2\text{)}$$

and

$$H - H_f < 50 \text{ Btu/lb} \quad .$$

The velocity term is identical with that of Eq. (8) and, within the prescribed limits, largely compensates for the inverse mass-velocity effect in the low-subcooling, low-quality region. These data and those of Gunther are unusually coherent, and the pronounced divergence of the subcooling dependencies, as will be discussed later, are only partially resolvable.

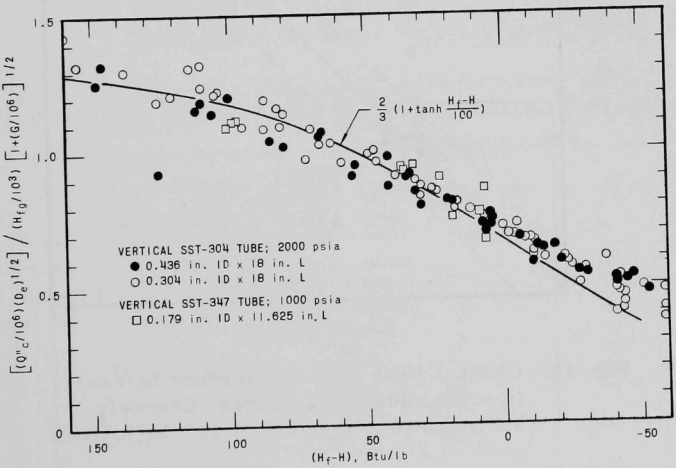

Fig. 17. Comparison of 1958 ANL Critical Heat Flux Data with Eq. (9) for $G > 0.90 \times 10^6$ lb/(hr)(ft^2).

At velocities below the arbitrary limit prescribed for Eq. (9), the flow-stream-velocity turbulence apparently contributes a relatively minor supplementation to the nucleate-boiling turbulence effect, and the forced-convection determinants of mass velocity and equivalent diameter no

longer appear as significant factors. Figure 18 presents a comparison of data for a comparatively wide range of pressures and flow geometry and size in the form:

$$Q_c''/10^6 = (H_{fg}/10^3)\left[1.75 + \frac{2}{3}\left(\frac{H_f - H}{100}\right)\right] \quad , \tag{10}$$

for

$$G < 0.90 \times 10^6 \text{ lb/(hr)(ft}^2\text{)} \quad .$$

These data show a comparatively low sensitivity to subcooling, comparable with that of the simple nucleate-boiling regime.

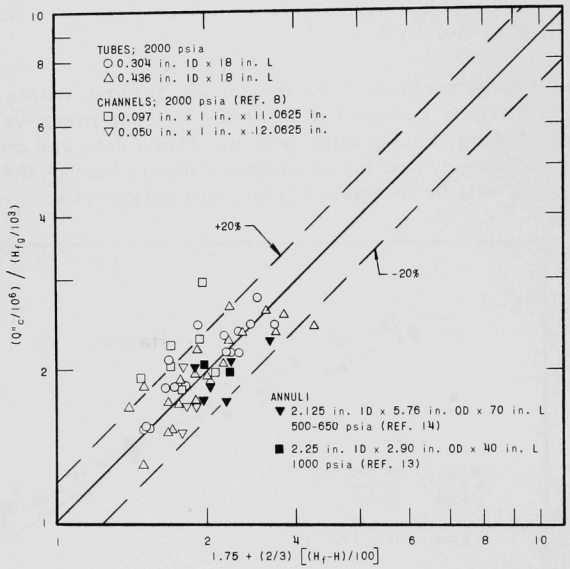

Fig. 18. Critical Heat Flux Occurrence in Vertical Stainless Steel Tubes, Channels, and Annuli for $G < 0.90 \times 10^6$ lb/(hr)(ft^2).

Figure 19 compares the "high" UCLA and Purdue data, the 1954 ANL data from stainless steel surfaces, and low-pressure KAPL data with Eqs. (8) and (9). A pressure dependency is apparent, the data at pressures of 500 psi and below following the linear subcooling behavior of Eq. (8) and the 1000-2000 psi data conforming to Eq. (9).

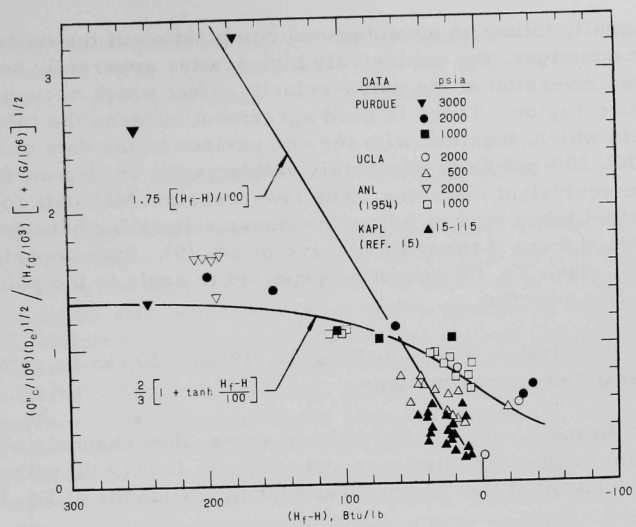

Fig. 19. Comparison of Experimental Data with Eqs. (8) and (9), Showing Effect of System Pressure on Critical Heat Flux Subcooling Dependency for Small Stainless Steel Tubes.

Figure 20 compares a wide range of the diameter variable with Eqs. (8) and (9). The Columbia data for large stainless steel tubes and

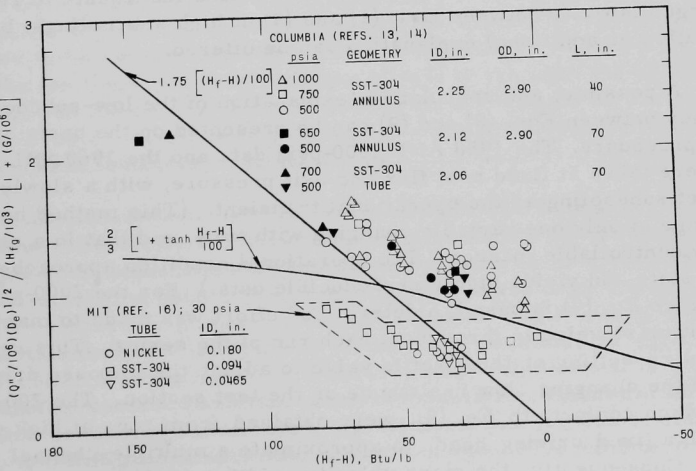

Fig. 20. Comparison of Experimental Data with Eqs. (8) and (9), Showing Effect of Geometry and Size Factors on Critical Heat Flux Subcooling Dependency.

annuli generally follow an advantageous combination of the subcooling factor of both equations, the excessively high scatter apparently being caused by a decided inversion of the mass-velocity effect which occurs well within the subcooled region. There is good agreement between the tubular and annular data which, together with the comparison of the data of Gunther with the ANL 200-psi data, adequately validates the boiling-surface evaluation of the equivalent diameter. The low-pressure MIT data for small stainless steel tubes tend to follow the linear subcooling behavior, departing upward from it toward the curve of Eq. (9). Such departure is to be expected, since Eq. (8) cannot be expected to apply to the point of zero subcooling and heat flux.

The data trends shown in Figs. 16, 19, and 20 can be summarized in the generalized approximations:

(1) At pressures of 1000 psi and above, flow channels of larger ($D_e \approx 1/8$ in. or greater) diameter and realistic L/D (>40) with good nucleating surfaces follow the critical heat flux behavior of Eq. (9).

(2) At lower pressures (500 psi or below), or for smaller flow channels, the critical heat flux follows the linear subcooling dependency of Eq. (8). (Nucleating surface requirements are indeterminate here, and no L/D limitation is apparent.)

(3) The higher-valued region of Eq. (8) is validated only by data from channels of low L/D. The increased thermal efficiency due to thermal and/or hydraulic entrance effects seems inadequate to reconcile the large disparity between Eqs. (8) and (9) at high subcoolings, but no alternative or additional explanation can be offered.

A possible, and speculative, explanation of the low-subcooling discrepancy between Eqs. (8) and (9) can be presented on the basis of operational procedure. The 1958 ANL 2000-psia data and the 1960 ANL 200-psia data were taken at fixed heat flux and exit pressure, with a slowly decreasing inlet subcooling as the operational transient. (This method has the advantage of only one variable changing with time, and that in a slow and readily controllable manner. The operational condition approaches that of steady state and yields highly reproducible data.) For the 2000-psia data, upon which Eq. (9) is based, a determined effort was made to maintain a constant mass velocity throughout each run of the series. This required frequent re-setting of the throttle valve to adjust the imposed driving head to the changing flow resistance of the test section. The 200-psia data, which conform to Eq. (8), were obtained from runs at high velocity and with a fixed driving head, to approximate a multiple-channel condition. Consequently, the mass velocity existing at the time of the critical heat flux occurrence was determined by the initial throttle-valve

setting and any subsequent enthalpy-induced changes in the flow resistance of the test section. The constant mass-velocity data are higher in value than the constant-pressure-drop 200-psia data.

V. DISCUSSION AND CONCLUSIONS

In axial-flow water systems, the simple nucleate-boiling flow regime exists only at the higher subcoolings [$(H_f - H) > 50$], the nucleate bubbles being quenched by the liquid flow stream. In addition to an adequate liquid-vapor temperature difference, effective bubble quenching requires flow channels of sufficient length and diameter that neither the hydraulic and/or thermal entrance effects nor the radial volume of the flow stream prevents dispersion of the bubbles into the flow stream. The system pressure and transfer-surface condition control the size and number of bubbles, and the equivalent diameter determines the radial dispersal volume of the flow stream; the unresolved relationship between bubble size and required dispersal volume necessitates the use of empirical limits for the determining conditions of this and other subcooled flow regimes. For system pressures of 500 psi or greater, mass velocity not appreciably less than 0.9×10^6 lb/(hr)(ft^2), and $D_e > \frac{1}{8}$ in., the simple nucleate-boiling critical heat flux occurrence has a low sensitivity to subcooling, a greater dependence on the transfer-surface condition, and is predictable by the modified convective heat transfer criteria of Eqs. (7) and (9).

Subject to the same limitations, Eqs. (7) and (9) also apply to the stratified bubble-flow regime which exists in the low-subcooling, low-steam-quality region. In this flow regime, the unquenched bubbles are considered to be concentrated in a sub-boundary layer which actively inhibits the frictional and heat transfer effects of the nucleate-boiling turbulence, and the critical heat flux shows no dependence on the surface condition, a major influence of subcooling, and a progressive decrease and inversion of the mass-velocity effect.

At low subcoolings and low mass velocity, the flow-stream turbulence neither effectively supplements the nucleate-boiling turbulence nor concentrates the unquenched bubbles about the flow-stream periphery. In this non-stratified bubble-flow regime, the critical heat flux has a low sensitivity to subcooling, similar to the simple nucleate-boiling flow regime, and is effectively independent of the mass-velocity and equivalent-diameter criteria of the convective heat transfer mechanism. The effect of the transfer-surface condition is not demonstrable, but the predominance of the nucleate-boiling turbulence suggests a surface influence. Within the accuracy and limitations specified, Eq. (10) predicts the critical heat flux occurrence in the non-stratified bubble-flow regime. It should be obvious that the distinction between these two regimes of bubble flow is a matter of degree rather than of the empirical delineation given, the stratified regime gradually changing to non-stratified flow as the concentration of bubbles about the flow-stream periphery decreases with decreasing velocity.

At low subcoolings and with flow channels less than $\frac{1}{8}$ in. in diameter, or pressures below 500 psi, a third form of bubble flow occurs. The required conditions suggest an appreciable population of unquenched bubbles whose aggregate size is large in comparison with the available dispersal volume; the resulting high void fraction conforms to descriptions of froth flow. In this flow regime, the critical heat flux shows an acute sensitivity to subcooling and follows the modified convective criteria of Eq. (8), with little or no indication of any inversion of the mass-velocity effect. A minor effect of surface condition was observed in the ANL 200-psi data.

As previously stated, the high subcooling range of Eq. (8) appears to be validated only by data from flow channels with low values of L/D_e. The nondetachment of bubbles from the boiling transfer surface observed by Gunther[11] in this region, which is probably due to the low values of the excess pressure characteristic (see Fig. 2) at low pressures, differs from the sub-boundary orientation of the stratified bubble-flow regime, as does the more acute subcooling dependency of the critical heat flux and the noninversion of the mass-velocity effect. (This latter occurrence is readily accounted for on the basis of bubble retention by the hydrodynamic boundary layer.) Gunther credits the additional boundary-layer turbulence which results from the bubbles retained therein for the abnormally high heat fluxes attained in the region of high subcooling. This explanation, plus the beneficial effects of entrance turbulence shown by the data of Bergles and Rohsenow,[16] is possibly sufficient to explain the large discrepancy in critical heat flux at high subcoolings between the simple nucleate boiling regime and the boundary-layer bubble-flow regime typified by the data of Gunther.

Subdivision of the recognized subcooled bubble-flow region into the four classifications noted is justified on the basis of observed changes in the heat transfer, flow friction, and critical heat flux. At the high intensities of nucleate boiling considered, the hypothesized causes are considered to be adequate and reasonable. The direct proportionality between the critical heat flux and the latent heat of vaporization appears to be a basic relationship for all nucleate boiling, both subcooled and net steam generation; it is believed that this same relationship applies to coolants other than water. The empirical inverse square root of the equivalent-diameter relationship is valid over a wide range of this variable and is believed to be extensible to coolants of low thermal conductivity other than water. Its applicability in the wet-steam region beyond "bubble flow" is questionable. The empirical approximations used for the subcooling and mass-velocity terms, as well as the empirical limitations used for the several projected divisions of bubble flow, are in need of refinement as better and more complete information becomes available.

REFERENCES

1. Forster, K. E., and Grief, R., Heat Transfer to a Boiling Liquid; Mechanism and Correlations, ASME Preprint 58-HT-11, Chicago (1958).

2. Bonjour, E., Verdier, J., and Weil, L., Improvement of Heat Exchanges in Boiling Liquids under the Influence of an Electric Field, AIChE Print 7, Houston (1962).

3. Jens, W. H., and Lottes, P. A., Analysis of Heat Transfer, Burnout, Pressure Drop, and Density Data for High-pressure Water, ANL-4627 (1951).

4. Berenson, P. J., Transition Boiling Heat Transfer, AIChE Preprint 18, Buffalo (1960).

5. Zuber, N., Hydrodynamic Aspects of Boiling Heat Transfer, AECU 4439 (1959).

6. Zuber, N., and Tribus, M., Further Remarks on the Stability of Boiling Heat Transfer, AECU 3631 (1958).

7. Weatherhead, R. J., and Lottes, P. A., Burnout Newsletter No. 1, BNL-2097 (1954).

8. DeBortoli, R. A., et al., Forced Convection Heat Transfer Burnout Studies for Water in Rectangular Channels and Round Tubes at Pressures above 500 psia, WAPD-188 (1958).

9. Silvestri, M., "Two-phase Flow and Heat Transfer," International Developments in Heat Transfer, ASME (1961) pp. 341-353.

10. Sher, H. C., Estimation of Boiling and Non-boiling Pressure Drop in Rectangular Channels at 2000 psia, WAPD-TH-300 (1957).

11. Gunther, F. C., Photographic Study of Surface-boiling Heat Transfer to Water with Forced Convection, Trans. ASME, 73, 115-123 (1951).

12. Epstein, H. M., et al., Heat Transfer and Burnout to Water at High Subcritical Pressures, BMI-1116 (1956).

13. Matzner, B., Basic Experimental Studies of Boiling Fluid Flow and Heat Transfer at Elevated Pressures, TID-16813 (Aug 1962).

14. Begell, W., Burnout Studies for the DuPont Power Reactor - Summary Report, AECU-4148 (1959).

15. Longo, J., A Statistical Investigation of Subcooled Burnout with Uniform and Locally Peaked Heat Fluxes, KAPL-1744 (1957).

16. Bergles, A. E., and Rohsenow, W. M., Forced Convection Surface Boiling Heat Transfer and Burnout in Tubes of Small Diameter, NP 11831 (1962).

APPENDIX

TABULATION OF 1958 ANL CRITICAL HEAT FLUX DATA

Table I

CRITICAL HEAT FLUX DEPENDENCY FOR A 0.304-in.-ID, TYPE 304 STAINLESS STEEL VERTICAL TUBE, 18-in. LONG, AT 2000 psia

Run No.	Q", 10^6 Btu/(hr)(ft^2)	G, 10^6 lb/(hr)(ft^2)	Inlet Subcooling,* Btu/lb	Exit Enthalpy Difference,** Btu/lb
8-53	1.70	1.89	299	-86.5
-54	1.42	1.93	223	-49
-55	1.29	2.00	184	-31.5
-56	1.14	1.97	155	-17
-57	0.995	1.95	118	4.5
-58	0.855	1.91	91	15.5
-59	0.720	1.88	63	27
-60	0.580	1.93	27	44.5
-61	1.67	1.95	284	-81.5
-62	1.44	1.95	221	-46.5
-63	1.23	1.99	170	-23.5
-64	1.14	1.98	155	-17.5
-65	1.00	1.96	119	2
-66	0.865	1.92	96	11
-67	0.715	1.89	62	28
-68	0.570	1.96	28	41
8-69†	1.62	1.48	364	-103.5
-70	1.43	1.50	295	-69.5
-71	1.27	1.49	248	-46
-72	1.14	1.48	214	-30
-73	0.990	1.46	167	-6.5
-75	0.865	1.50	125	12
-76	0.715	1.46	86	30
-77	0.571	1.50	47	44
-78	0.480	1.48	17	60
-79†	1.63	1.47	372	-109.5
8-34	1.65	1.23	426	-109.5
-35	1.37	1.22	347	-81
-36	1.29	1.22	317	-66.5
-37	1.15	1.28	251	-38.5
-38	0.980	1.25	197	-11.5
-39	0.840	1.24	151	8
-40	0.740	1.24	117	23.5
-41	0.595	1.22	74	42

*$\Delta h_{sub} = h_{sat} - h_{in}$ **$\Delta h_{sat} = h_{ex} - h_{sat}$

†Howling in test section.

Table I (Contd.)

Run No.	Q", 10^6 Btu/(hr)(ft^2)	G, 10^6 lb/(hr)(ft^2)	Inlet Subcooling,* Btu/lb	Exit Enthalpy Difference,** Btu/lb
8-42	0.498	1.19	39	60
-43†	1.64	1.23	428	-113.5
-44	1.42	1.22	356	-80
-45	1.29	1.23	310	-62.5
-46	1.14	1.23	256	-35.5
-47	1.00	1.24	207	-16.5
-48	0.840	1.24	151	10
-49	0.715	1.24	112	25
-50	0.572	1.22	67	44
-51	0.484	1.18	35	62
-52	0.458	1.20	17	73.5
7-1	1.15	0.985	349	-72
-2	0.855	0.951	207	5
-3	1.425	1.03	452	-126
-4	1.13	0.996	327	-59
-5	0.855	0.960	200	11
-6	0.735	0.972	137	42.5
-7	0.573	0.990	85	51.5
-8	0.430	1.00	21	81.5
-9	1.57	1.08	480	-138
-10	1.29	1.02	385	-87
-11	1.00	1.04	258	-30
-12	0.860	1.01	196	5.5
-13	0.715	1.02	129	37
-14	0.565	1.00	74	60
-15	0.485	1.02	41	71
-16	0.425	0.987	16	86.5
-30	1.69	1.01	556	-159.5
-31	1.43	1.00	441	-105
8-1	1.57	1.00	525	-155
-2	1.43	1.01	456	-121
-3	1.30	1.00	400	-105.5
-5	1.02	0.998	268	-26.5
-6	0.855	1.02	198	0.5
-7	0.715	1.02	144	22.5
-8	0.580	1.00	96	41.5
-9	0.440	0.900	27	89.5

Table I (Contd.)

Run No.	Q", 10^6 Btu/(hr)(ft^2)	G, 10^6 lb/(hr)(ft^2)	Inlet Subcooling,* Btu/lb	Exit Enthalpy Difference,** Btu/lb
8-17	1.28	0.710	544	-117.5
-19	1.00	0.705	404	-65.5
-20	0.860	0.687	299	-2
-21	0.720	0.683	216	34
-22	0.545	0.673	112	79.5
-23	0.480	0.673	68.5	100.5
-24	0.434	0.690	42.5	102.5
-25	1.29	0.690	557	-116.5
-26	1.14	0.705	489	-105
-27	1.00	0.695	407	-65.5
-28	0.860	0.685	306	-10
-29	0.707	0.682	208	37
-30	0.570	0.685	119	77
-31	0.485	0.685	68.5	98.5
-32	0.431	0.696	42.5	104.5
-33	0.386	0.656	10	129
7-17	1.14	0.512	556	-26.5
-18	1.00	0.541	524	-85
-19	0.860	0.511	391	6
-20	0.685	0.495	266	62.5
-21	1.10	0.545	565	-84.5
-22	1.08	0.520	554	-62.5
-23	0.975	0.491	460	9
-24	0.860	0.500	391	14
-25	0.715	0.485	273	77
-26	0.550	0.491	147	117
-27	0.488	0.511	94	130
-28	0.435	0.496	66	142.5
-29	0.370	0.470	4.5	182
8-10	1.00	0.508	538	-72.5
-12	0.715	0.520	295	31.5
-13	0.572	0.500	192	78
-14	0.484	0.491	105	127.5
-15	0.430	0.480	71.5	140.5
-16	0.370	0.466	20	167

Table II

CRITICAL HEAT FLUX DEPENDENCY FOR A 0.304-in.-ID, TYPE 304 STAINLESS STEEL VERTICAL TUBE, 18-in. LONG, AT 2000 psia

Run No.	Q", 10^6 Btu/(hr)(ft^2)	G, 10^6 lb/(hr)(ft^2)	Inlet Subcooling,* Btu/lb	Exit Enthalpy Difference,** Btu/lb
18-1†	1.26	1.55	514	-380
-2†	1.13	1.51	401	-277.5
-3†	1.04	1.53	237	-126
-4†	0.954	1.47	149	-42
-5	0.838	1.47	98	-4.5
-6	0.741	1.47	77	6
-7	0.639	1.45	61.5	10.5
-8	0.559	1.35	26.5	41
-18	1.24	1.42	250	-106
-19	1.14	1.44	197	-67
-20	0.997	1.48	145	-34
-21	0.897	1.47	120	-20
-22	0.800	1.47	97	-7.5
-23	0.709	1.44	68.5	12.5
-24	0.583	1.40	37.5	31
-25	0.536	1.33	25	41
-36	1.32	1.48	246	-99.5
-37	1.19	1.52	195	-65.5
-38	1.085	1.50	162	-42.5
-39	1.075	1.50	160	-41.5
-40	0.997	1.50	145	-35.5
-41	0.897	1.49	118	-18.5
-42	0.804	1.51	91.5	-4.5
-43	0.705	1.51	62.5	14.5
-44	0.595	1.44	40.5	27.5
-45	0.499	1.30	10	53
18-9	1.24	0.991	353	-147.5
-10	1.14	0.978	303	-111.5
-11	1.03	0.995	256	-85
-12	0.937	1.00	207	-54
-13	0.837	0.992	170	-31.5
-14	0.734	0.990	127	-4.5
-15	0.638	0.991	87.5	18.5
-16	0.522	0.991	39	47.5

*$\Delta h_{sub} = h_{sat} - h_{in}$ **$\Delta h_{sat} = h_{ex} - h_{sat}$

†Runs 18-1, 2, 3, and 4 are excellent examples of the effect of surface condition.

Table II (Contd.)

Run No.	Q", 10^6 Btu/(hr)(ft^2)	G, 10^6 lb/(hr)(ft^2)	Inlet Subcooling,* Btu/lb	Exit Enthalpy Difference,** Btu/lb
18-17	0.443	0.885	8.5	73.5
-26	1.30	0.991	361	-146
-27	1.165	0.980	305	-109.5
-28	1.10	1.01	292	-111.5
-29	1.01	1.00	246	-79.5
-30	0.897	1.00	202	-54.5
-31	0.794	1.01	160	-30
-32	0.699	1.04	117	-6.5
-33	0.586	1.03	73	21
-34	0.505	1.01	37.5	45
-35	0.405	0.795	6.5	77
18-46	1.22	0.514	524	-134
-47	1.10	0.506	446	-90
-48	1.02	0.496	362	-25
-49	0.914	0.506	320	-24
-50	0.885	0.502	296	-6
-51	0.790	0.505	260	-3
-52	0.702	0.506	223	5.5
-53	0.600	0.497	162	37
-54	0.499	0.513	87.5	72.5
-55	0.415	0.496	28.5	108.5
-56	0.382	0.449	5.5	134.5
-57	1.24	0.500	477	-71
19-1	1.13	0.509	595	-229
-2	1.20	0.509	552	-166
-3	1.10	0.507	508	-152
-4	1.06	0.496	420	-70.5
-5	0.958	0.491	382	-62
-6	0.902	0.487	343	-39
-7	0.801	0.496	287	-22
-8	0.700	0.508	217	10
-9	0.602	0.503	159	38
-10	0.499	0.508	81	84
-11	0.406	0.508	25	110
19-12	0.818	0.245	481	68
-13	0.761	0.251	424	76.5
-14	0.672	0.246	332	117.5
-15	0.575	0.252	245	130
-16	0.473	0.252	140	168

Table II (Contd.)

Run No.	Q", 10^6 Btu/(hr)(ft^2)	G, 10^6 lb/(hr)(ft^2)	Inlet Subcooling,* Btu/lb	Exit Enthalpy Difference,** Btu/lb
19-17	0.417	0.262	78	182
-18	0.369	0.274	42.5	179.5
-19	0.330	0.256	5.5	206.5
-20	0.858	0.251	525	36
-21	0.781	0.250	464	51
-22	0.702	0.250	387	74
-23	0.670	0.255	327	105
-24	0.612	0.254	279	117.5
-25	0.549	0.256	204	147.5
-26	0.499	0.253	157	166
-27	0.475	0.266	126.5	166.5
-28	0.432	0.262	91.5	179.5
-29	0.373	0.260	42.5	193.5
-30	0.339	0.251	5.5	216.5
-31	0.880	0.258	601	-39.5
-32	0.801	0.255	510	8
-34	0.599	0.240	281	129.5
-35	0.489	0.254	152	164
-36	0.400	0.262	64	187
-37	0.320	0.250	0	210
19-38	0.499	0.147	499	58
-39	0.500	0.140	489	96
-40	0.480	0.149	443	87
-41	0.415	0.136	311	189.5
-42	0.383	0.140	173	276.5
-43	0.381	0.152	138	274.5
-44	0.349	0.135	128	296.5
-45	0.320	0.133	85	311
-46	0.279	0.136	26.5	309.5
-47	0.279	0.138	15.5	318.5
-48	0.509	0.155	500	36
-49	0.462	0.154	446	44
-50	0.450	0.154	422	59.5
-51	0.435	0.151	386	88
-52	0.423	0.141	311	180.5
-53	0.410	0.140	222	263.5
-54	0.383	0.140	170	281
-55	0.359	0.146	130	274
-56	0.355	0.144	120	287

Table II (Contd.)

Run No.	Q", 10^6 Btu/(hr)(ft^2)	G, 10^6 lb/(hr)(ft^2)	Inlet Subcooling,* Btu/lb	Exit Enthalpy Difference,** Btu/lb
19-57	0.316	0.140	75.5	294.5
-58	0.303	0.138	61	301
-59	0.296	0.126	54.5	331.5
-60	0.280	0.138	48.5	283.5
-61	0.259	0.132	42.5	281.5
-62	0.495	0.144	470	94
-63	0.463	0.148	413	101.5
-64	0.440	0.152	357	118.5
-65	0.399	0.135	241	244.5
-66	0.390	0.138	183	282
-67	0.370	0.145	140	280
-68	0.345	0.136	117	298.5
-69	0.315	0.134	83.5	301.5
-70	0.275	0.126	31.5	326.5